

## Terahertz surface plasmon propagation in nanoporous silicon layers

Shu-Zee A. Lo<sup>a)</sup> and Thomas E. Murphy<sup>b)</sup>

*Department of Electrical & Computer Engineering, Institute for Research in Electronics & Applied Physics, University of Maryland, College Park, Maryland 20740, USA*

(Received 10 March 2010; accepted 29 April 2010; published online 18 May 2010)

We describe the fabrication and measurement of a terahertz surface plasmon waveguide in which the optical mode is localized within a nanoporous silicon slab. We compare the propagation characteristics among waveguides with different porous layer thickness, and present an analytical model that accurately describes the dispersion and loss in the waveguides. © 2010 American Institute of Physics. [doi:10.1063/1.3432071]

Terahertz (THz) surface plasmon waveguides have attracted interest because of their unique ability to support low-loss THz modes that are localized near the surface of a semiconductor or metal.<sup>1–6</sup> Surface plasmon waveguides have been explored for use in THz modulators,<sup>7</sup> quantum cascade lasers,<sup>8</sup> near-field optics,<sup>9–11</sup> and sensors,<sup>12</sup> all of which benefit from the tight mode confinement near a surface.

The characteristics of a surface plasmon wave are strongly modified by the presence of a dielectric film on the surface—an effect that has been exploited and commercialized to achieve optical sensors capable of detecting even monolayer films.<sup>13</sup> However, it is difficult to achieve this sensitivity in the THz regime, where a monolayer film is negligibly thin in comparison to the size of a typical THz surface plasmon mode. The effect of dielectric layers on THz surface plasmons has been investigated using gold films coated with cyclotene,<sup>14</sup> copper wires coated with polyurethane,<sup>15</sup> silver covered with epitaxially grown films of intrinsic silicon,<sup>16</sup> and in InSb semiconductor wafers coated with films of polystyrene.<sup>17</sup>

In this paper, we describe a THz surface plasmon waveguide that incorporates a nanoporous dielectric layer above a highly-doped silicon substrate. In contrast with earlier studies, the porous layer reported here allows a very large internal surface area to be distributed throughout a volume that is comparable in size to the THz wavelength. This structure could have important advantages in THz sensing, spectroscopy, and applications that rely on surface modification or selective surface binding. We present here an experimental characterization of a surface plasmon wave in nanoporous silicon layers, together with an analytical model that predicts the dispersion and loss for nanoporous films of different thickness.

Porous silicon is a nanoscale composite of silicon and air that is formed by electrochemical etching of crystalline silicon. The porosity and average pore dimension formed in this process depend on doping concentration of the substrate and the electrochemical etching current, which can be controlled during fabrication to make thick multilayer structures. It has been previously shown that, despite being formed from a doped substrate, porous silicon can behave like a low-loss transparent dielectric at THz frequencies.<sup>18,19</sup> Moreover, as

we show here, the doped silicon substrate below the porous layer can serve as a convenient, mechanically robust, conducting medium for supporting a surface plasmon mode.

The porous silicon layers were fabricated from p<sup>+</sup> silicon wafers with a boron dopant concentration of 10<sup>19</sup> cm<sup>-3</sup> and a corresponding resistivity of 5 mΩ cm. Electrochemical etching was carried out in a solution of hydrofluoric acid, water, and ethanol in 1:1:2 volume ratio, with an electrochemical current density of 90.7 mA/cm<sup>2</sup> applied in 100 ms pulses with 300 ms intervening pauses, using a twin-chamber electrochemical cell.<sup>19</sup> Using gravimetric and profilometric measurements, we determined the porosity to be 62% under these etching conditions. The corresponding refractive index at THz frequencies was estimated to be 1.67, from Fabry–Pérot measurements of a free-standing porous layer fabricated under similar conditions.<sup>20</sup> For the surface plasmon waveguides considered here, we fabricated three samples with porous layers of 10.6, 28.3, and 56.4 μm thickness. Figure 1(a) shows a cross-sectional micrograph of the 10.6 μm film on the silicon substrate, with enlarged views showing the nanoporous structure.

We adopted the aperture coupling technique to excite THz surface plasmon waves, as shown in Fig. 1(b).<sup>14</sup> While this method has lower efficiency compared to grating coupling, it allows for broadband coupling which is desirable for

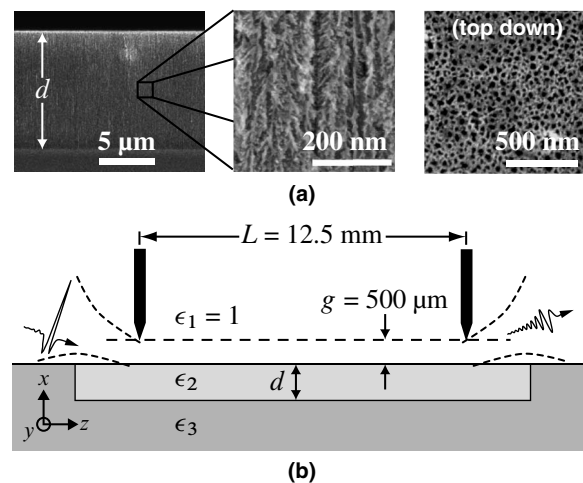


FIG. 1. (a) Scanning electron micrographs of a 10.6 μm porous silicon layer on a doped silicon substrate. The enlarged micrographs show the nanoscale structure of the porous skeleton. (b) Diagram showing aperture coupling technique used to couple THz radiation into and out of the surface plasmon waveguide.

<sup>a)</sup>Electronic mail: alenciou@umd.edu.

<sup>b)</sup>Electronic mail: tem@umd.edu.

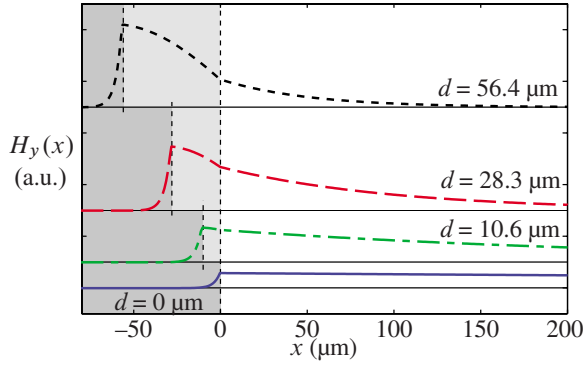


FIG. 2. (Color online) Calculated transverse magnetic field profiles for the surface plasmon modes of a nanoporous silicon waveguide. The lowest curve shows the surface plasmon mode of a silicon wafer with no porous layer, and the upper three curves correspond to waveguides with porous layers with thickness 10.6, 28.3, and 56.4  $\mu\text{m}$ . All modes were calculated at a frequency of 1 THz, and normalized to have the same total power.

spectroscopy measurements. THz pulses were generated by illuminating an InAs semiconductor surface with 120 fs pulses from a Ti-sapphire oscillator operating at 810 nm. The emitted THz signal was collimated and focused from free-space onto the input aperture at an angle of  $80^\circ$  from the surface normal. The razor blades were spaced 500  $\mu\text{m}$  away from the sample surface, and the THz beam was focused to a spot-size of approximately 2 mm. The output blade was located 12.5 mm away from the input aperture. The emerging signal was collimated and focused onto the surface of a zinc-telluride electro-optic detector. The THz signal generated by this system exhibits a detectable spectrum between 0.1 and 2.5 THz. For the measurements reported here, we aligned the experiment to ensure that the incident THz wave was TM-polarized (transverse magnetic field) with respect to the sample surface. When the input wave was instead TE-polarized (transverse electric field), there was no measurable transmitted signal, as expected.

The TM surface plasmon mode of the three-layer asymmetric waveguide can be expressed in the following form:<sup>21</sup>

$$H_y(x) = \begin{cases} H_0 e^{-\kappa_1 x}, & 0 < x \\ H_0 \left( \cos \kappa_2 x - \frac{\epsilon_{2\parallel} \kappa_1}{\epsilon_1 \kappa_2} \sin \kappa_2 x \right), & -d < x < 0 \\ H_0 \left( \cos \kappa_2 d + \frac{\epsilon_{2\parallel} \kappa_1}{\epsilon_1 \kappa_2} \sin \kappa_2 d \right) \\ \times e^{\kappa_3(x+d)}, & x < -d \end{cases}, \quad (1)$$

where  $H_0$  is a normalization constant, typically chosen such that the mode carries unity power. The variables  $\kappa_1$ ,  $\kappa_2$ , and  $\kappa_3$  are given by

$$\kappa_1^2 \equiv \beta^2 - \epsilon_1 k^2, \quad (2)$$

$$\kappa_2^2 \equiv \epsilon_{2\parallel} k^2 - \sigma^2 \beta^2, \quad (3)$$

$$\kappa_3^2 \equiv \beta^2 - \epsilon_3 k^2, \quad (4)$$

where  $\beta$  is the complex propagation constant of the mode,  $k \equiv \omega/c$  is the vacuum wave vector, and  $\sigma^2 \equiv \epsilon_{2\parallel} / \epsilon_{2\perp}$  is a ratio describing the anisotropy of the middle layer.

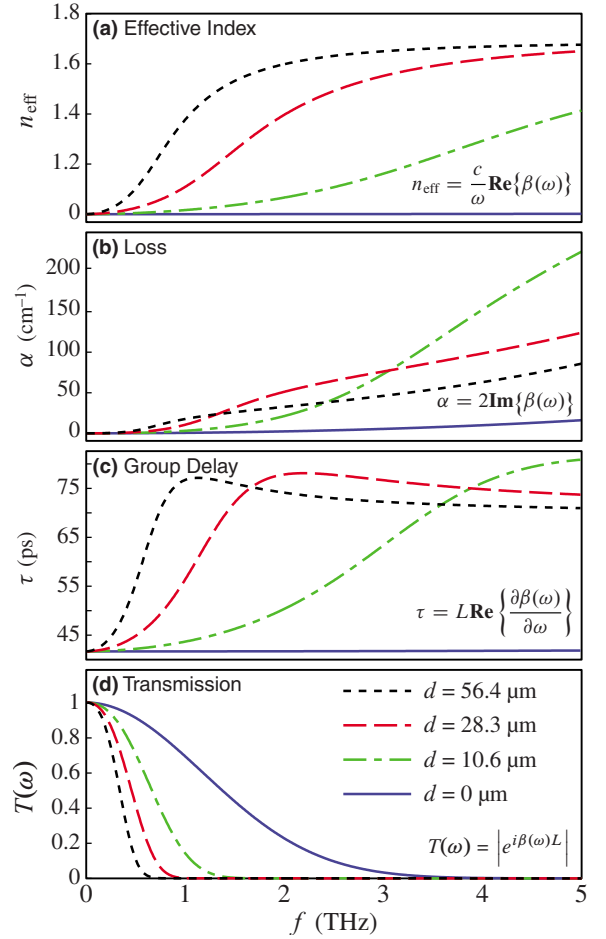


FIG. 3. (Color online) (a) Calculated effective index and (b) attenuation factor as a function of frequency. (c) Calculated group delay and (d) amplitude transmission spectrum for a 12.5 mm long waveguide. In each case, the four curves shown correspond to porous layer thicknesses of 0, 10.6, 28.3, and 56.4  $\mu\text{m}$ .

By matching the boundary conditions at  $x=0$  and  $x=-d$ , one obtains the following dispersion relation for the plasmon mode,

$$kd = \sqrt{\frac{1}{\epsilon_{2\parallel} - \sigma^2 \epsilon_{\text{eff}}}} \left[ \tan^{-1} \left( \frac{\epsilon_{2\parallel}}{\epsilon_1} \sqrt{\frac{\epsilon_{\text{eff}} - \epsilon_1}{\epsilon_{2\parallel} - \sigma^2 \epsilon_{\text{eff}}}} \right) + \tan^{-1} \left( \frac{\epsilon_{2\parallel}}{\epsilon_3} \sqrt{\frac{\epsilon_{\text{eff}} - \epsilon_3}{\epsilon_{2\parallel} - \sigma^2 \epsilon_{\text{eff}}}} \right) \right], \quad (5)$$

where  $\epsilon_{\text{eff}} \equiv (\beta/k)^2$ .

In Fig. 2 we plot the calculated transverse magnetic field of the surface plasmon mode for porous layer thicknesses of 0, 10.6, 28.3, and 56.4  $\mu\text{m}$ . These modes were calculated at a frequency of 1.0 THz, and all are normalized to have the same optical power. In all cases, the surface plasmon mode reaches its maximum value at the interface between the substrate and the porous silicon layer. The propagation loss of the mode is strongly related to the mode intensity at the lossy silicon surface, which depends on the film thickness.<sup>16</sup> The modes decay evanescently in the air region, with  $1/e$  penetration depths of 1,820  $\mu\text{m}$ , 900  $\mu\text{m}$ , 410  $\mu\text{m}$ , and 200  $\mu\text{m}$ , for the 0  $\mu\text{m}$ , 10.6  $\mu\text{m}$ , 28.3  $\mu\text{m}$ , and 56.4  $\mu\text{m}$  cases, respectively. We note that the field penetration depth will influence the coupling at the input and output apertures but we did not include this effect in our simulations.

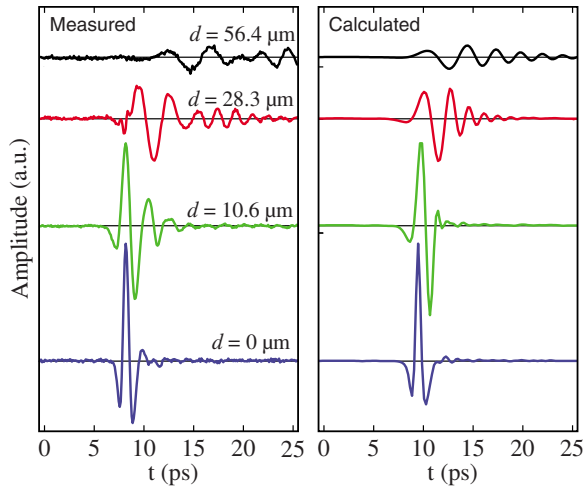


FIG. 4. (Color online) Comparison of measured (left) and calculated (right) time domain traces for the four different surface plasmon waveguides considered here.

To numerically calculate the propagation of the plasmon mode, we modeled the dielectric layer by  $\epsilon_{21}=1.67^2$  and we neglected the (unmeasured) anisotropy of the porous layer by letting  $\sigma=1$ . The dielectric constants of the doped silicon substrate were approximated using a simple Drude model,

$$\epsilon_3(\omega) = \epsilon_R - \frac{\omega_p^2}{\omega^2 - i\omega\gamma}, \quad (6)$$

where for p<sup>+</sup> silicon with resistivity of 5 mΩ cm, we estimate  $\omega_p/2\pi=19.9$  THz and  $\gamma/2\pi=12.7$  THz.

In Figs. 3(a) and 3(b), we plot the calculated effective refractive index of the surface plasmon mode and the corresponding attenuation constant  $\alpha(\equiv 2 \text{Im}\{\beta\})$  as a function of frequency, for porous waveguides with layer thicknesses of  $d=10.6, 28.3,$  and  $56.4 \mu\text{m}$ , together with the corresponding curves for a conventional silicon-air surface plasmon ( $d=0$ ). These curves were obtained by numerically solving Eq. (5). Figures 3(c) and 3(d) show how these dispersion curves are expected to affect the propagation through a 12.5 mm long waveguide. Figure 3(c) shows the calculated group delay for a 12.5 mm waveguide and Fig. 3(d) plots the predicted transmission through the 12.5 mm waveguide, taking into account the calculated frequency-dependent attenuation. When the film thickness is increased, the plasmon waveguide exhibits stronger group delay dispersion and increased loss at higher frequencies. These effects are primarily attributed to modal dispersion inherent in the solution to Eq. (5), rather than material dispersion arising from Eq. (6).

Figure 4 compares the measured THz time-domain response to that calculated theoretically from the dispersion characteristics of Fig. 3. The experimental traces were measured using the experimental setup depicted in Fig. 1. When calculating the theoretical response, we obtained a reference time-domain trace by realigning the optics to bypass the waveguide entirely, giving an unobstructed transmitted

waveform. We then fed this measured input signal into the calculated dispersion relation shown in Fig. 3 and numerically computed the expected time-domain traces after a propagation distance of 12.5 mm. Even though this method neglects the input and output coupling, the theoretically calculated traces show much the same behavior that we observed experimentally. In particular, it is seen that as the film thickness increases, modal dispersion plays an increasingly important role in spreading the pulses.

In conclusion, we describe the fabrication and measurement of a THz surface plasmon waveguide in which the THz mode is guided in a nanoporous silicon layer. We present calculations and measurements of the time-domain response that show the role of modal dispersion and frequency-dependent loss in the propagation. Because of the large internal surface area inherent to porous materials, this structure holds promise for sensor and spectroscopy applications that rely on selective surface binding.

This work was sponsored by the Office of Naval Research, through the University of Maryland Center for Applied Electromagnetics (Grant No. N000140911190) with the support of the Maryland NanoCenter and its NispLab and FabLab.

- <sup>1</sup>D. Begley, R. Alexander, C. A. Ward, and R. Bell, *Surf. Sci.* **81**, 238 (1979).
- <sup>2</sup>E. Koteles and W. McNeill, *Int. J. Infrared Millim. Waves* **2**, 361 (1981).
- <sup>3</sup>T.-I. Jeon and D. Grischkowsky, *Appl. Phys. Lett.* **88**, 061113 (2006).
- <sup>4</sup>J. O'Hara, R. Averitt, and A. Taylor, *Opt. Express* **13**, 6117 (2005).
- <sup>5</sup>K. Wang and D. M. Mittleman, *Nature (London)* **432**, 376 (2004).
- <sup>6</sup>A. Agrawal, H. Cao, and A. Nahata, *New J. Phys.* **7**, 249 (2005).
- <sup>7</sup>J. Gómez Rivas, M. Kuttge, H. Kurz, P. Haring Bolivar, and J. A. Sánchez-Gil, *Appl. Phys. Lett.* **88**, 082106 (2006).
- <sup>8</sup>R. Colombelli, F. Capasso, C. Gmachl, A. L. Hutchinson, D. L. Sivco, A. Tredicucci, M. C. Wanke, A. M. Sergent, and A. Y. Cho, *Appl. Phys. Lett.* **78**, 2620 (2001).
- <sup>9</sup>Y. B. Ji, E. S. Lee, J. S. Jang, and T. I. Jeon, *Opt. Express* **16**, 271 (2008).
- <sup>10</sup>S. Maier, S. Andrews, L. Martín-Moreno, and F. García-Vidal, *Phys. Rev. Lett.* **97**, 176805 (2006).
- <sup>11</sup>A. J. Huber, F. Keilmann, J. Wittborn, J. Aizpurua, and R. Hillenbrand, *Nano Lett.* **8**, 3766 (2008).
- <sup>12</sup>C. Rau, G. Torosyan, R. Beiganga, and K. Nerkararyan, *Appl. Phys. Lett.* **86**, 211119 (2005).
- <sup>13</sup>S. Y. Wu, H. P. Ho, W. C. Law, C. Lin, and S. K. Kong, *Opt. Lett.* **29**, 2378 (2004).
- <sup>14</sup>J. Saxler, J. G. Rivas, C. Janke, H. Pellemans, P. Bolívar, and H. Kurz, *Phys. Rev. B* **69**, 155427 (2004).
- <sup>15</sup>N. C. J. van der Valk and P. C. M. Planken, *Appl. Phys. Lett.* **87**, 071106 (2005).
- <sup>16</sup>K. W. Steijn, R. J. Seymour, and G. I. Stegeman, *Appl. Phys. Lett.* **49**, 1151 (1986).
- <sup>17</sup>T. H. Isaac, W. L. Barnes, and E. Hendry, *Appl. Phys. Lett.* **93**, 241115 (2008).
- <sup>18</sup>S. Labbé-Lavigne, S. Barret, F. Garet, L. Duvillaret, and J.-L. Coutaz, *J. Appl. Phys.* **83**, 6007 (1998).
- <sup>19</sup>S.-Z. A. Lo, A. M. Rossi, and T. E. Murphy, *Phys. Status Solidi A* **206**, 1273 (2009).
- <sup>20</sup>S.-Z. A. Lo and T. E. Murphy, *Opt. Lett.* **34**, 2921 (2009).
- <sup>21</sup>I. P. Kaminow, W. L. Mammel, and H. P. Weber, *Appl. Opt.* **13**, 396 (1974).